Electrochimica Acta 270 (2018) 138–146

Contents lists available at ScienceDirect

Electrochimica Acta

journal homepage: www.elsevier.com/locate/electacta

Synergistic effect of iron diselenide decorated multi-walled carbon nanotubes for enhanced heterogeneous electron transfer and electrochemical hydrogen evolution

Swagotom Sarker [a, 1], Pavan Chaturvedi [b, c, 1], Litao Yan [a], Tom Nakotte [a], Xinqi Chen [d], Stephanie K. Richins [a], Sanjib Das [e], Jonathan Peters [a, 2], Meng Zhou [a], Sergei N. Smirnov [b, *], Hongmei Luo [a, **]

[a] Department of Chemical and Materials Engineering, New Mexico State University, Las Cruces, NM 88003, USA
[b] Department of Chemistry and Biochemistry, New Mexico State University, Las Cruces, NM 88003, USA
[c] Department of Physics, New Mexico State University, Las Cruces, NM 88003, USA
[d] Northwestern University Atomic and Nanoscale Characterization Experimental (NUANCE) Center, Northwestern University, Evanston, IL 60208, USA
[e] Department of Materials Science and Engineering, Northwestern University, Evanston, IL 60208, USA

ARTICLE INFO

Article history:
Received 26 September 2017
Received in revised form
26 February 2018
Accepted 11 March 2018
Available online 12 March 2018

Keywords:
Hydrothermal synthesis
MWCNT
$FeSe_2$
Heterogeneous electron transfer
Hydrogen evolution reaction
Synergistic effect

ABSTRACT

Iron diselenide ($FeSe_2$) has been of recent interest as a potentially useful electrode material. Here we demonstrate, for the first time, the synergistic effect between multi-walled carbon nanotubes (MWCNT) and $FeSe_2$ in a form of MWCNT/$FeSe_2$ composite, for the heterogeneous electron transfer (HET) reaction with the $[Ru(NH_3)_6]^{3+/2+}$ redox probe and the electrochemical hydrogen evolution reaction (HER) in acidic media. Plain $FeSe_2$ and the MWCNT/$FeSe_2$ composite were synthesized using a one-pot hydrothermal method. Although all electrode materials (pristine MWCNT, $FeSe_2$, and MWCNT/$FeSe_2$) show a quasi-reversible electrode behavior, MWCNT/$FeSe_2$ has a smaller peak separation potential and exhibits an enhanced HET rate constant, $k^0 = 5.4 \times 10^{-3}$ cm/s, which is 3.2 and 1.6 times higher than that of $FeSe_2$ and MWCNT, respectively. Similarly, the HER performance of the composite demonstrates a smaller Tafel slope of 70 mV/dec and a reduced overpotential. We anticipate that such promising outcome can be further improved by employing different morphologies of $FeSe_2$ and engineered interaction with other conductive supports suitable for their applications in electrochemical sensing and energy conversion.

1.Introduction

Transition metal dichalcogenides (TMDCs) such as molybdenum disulfide (MoS_2), molybdenum diselenide ($MoSe_2$), iron diselenide ($FeSe_2$), and metal-free catalysts have recently generated much attention for their promising applications in electrochemical sensing [1], electrocatalysis [2–8], Li-ion & Na-ion batteries [9,10], cancer therapy [11], etc. In particular, numerous reports on various nanoarchitectures and morphologies of TMDCs [2,5,12] and their combination with different supportive materials [13–16] have demonstrated improved features in the applications to electrocatalytic hydrogen evolution reaction (HER). Hydrogen, a clean energy carrier with an energy density of 142 MJ/kg, can be produced via electrocatalysis [14,17], photocatalysis [18], and steam reforming [19]. Although electrocatalytic reduction of water is the most feasible way to produce hydrogen, its realistic implementation remains challenging due to the high cost of platinum, currently the best HER catalyst with the lowest overpotential [20,21]. As a result, significant research has been devoted to the development of the non-noble metal electrocatalysts including such from diverse and abundant TMDCs. The most studies have been focusing on MoS_2 due to its near zero hydrogen binding energy at the edges but other low-cost TMDC catalysts have not received enough attention for the application in HER and their behavior as electrodes is not

* Corresponding author.
** Corresponding author.
E-mail addresses: swagotom@nmsu.edu (S. Sarker), pavansnn@nmsu.edu (P. Chaturvedi), ramosyan@nmsu.edu (L. Yan), tnakotte@nmsu.edu (T. Nakotte), xchen@northwestern.edu (X. Chen), richins7@nmsu.edu (S.K. Richins), mzhou@nmsu.edu (M. Zhou), snsm@nmsu.edu (S.N. Smirnov), hluo@nmsu.edu (H. Luo).
[1] Equal contribution.
[2] Present address: National Nuclear Laboratory, Workington Laboratory, Derwent Howe, CA14 3YQ, UK.

https://doi.org/10.1016/j.electacta.2018.03.064
0013-4686/

well-understood [2,12,22].

Electrode kinetics can be better understood by studying HER with other heterogeneous electron transfer (HET) reactions, which are not only more convenient but also can identify applications of the electrode materials in sensing and electrocatalysis. HET performance strongly depends on the electronic structure of the electrode material such as: an overlap between its energy levels with those of the redox species [23–26] and the charge transfer through the electrode [25]; its morphology often plays a significant role. Carbon materials in the form of highly ordered pyrolytic graphite (HOPG) [27], single-walled carbon nanotubes [28], graphene [29,30], and hybrids of graphene with CNT [25,31,32] have been particularly attractive because of the rich possibilities of their frontier orbital energies, native morphology, and versatility of chemical and physical modifications. In particular, considerable research has been devoted to understand the kinetic activity of edges, basal planes, defects, and the role of multiple graphene layers [29,30,33,34]. The overall kinetics of a charge transfer reaction is controlled by the slowest step between the mass transport and the charge transfer. Introduction of nanoelectrodes or electrodes placed at nanometer-sized gaps can remarkably improve the HET behavior as a result of the enhanced mass transport [24,35]. For HOPG and graphene, it was reported that faster kinetics arise primarily at the edges rather than at the basal planes [27,30,36]; Velický et al. have found a great variation in the HET activity across the basal planes of mono- and multi-layered graphene [29]. Therefore, it is believed that the morphology of the electrode materials strongly affects its performance. At the same time, there has been growing interest in understanding the HET kinetics of the bulk and the layered structures of TMDCs [37–39]. Tan et al. demonstrated that the edges of MoS_2 also exhibit significantly enhanced HET and HER activity in comparison to its basal planes [40]. Improvement in the charge transfer rates can be further realized by introducing a conductive support such as carbon nanotubes [25,31]. Synergistic effect due to carbon nanotube incorporation has been reported in the design of electrodes for thiocyanate detection [41], glucose sensing [42], and hydrogen peroxide sensing [43].

As one of the TMDCs, $FeSe_2$ possesses a direct band gap of 1.0 eV [44] and a relatively good electrical conductivity [4]. A large abundance of iron and the expected high HER activity comparable to the metalloenzymes [45,46] make this material of a particular interest. It can be easily synthesized by electrodeposition [47], hydrothermal process [10], and selenization of iron oxide [48]. It is well-established that an increase in the number of the active sites and an introduction of a conductive support can enhance the electrocatalytic activity. For example, the HER activity of $FeSe_2$ and its composite with graphene oxide have been recently reported [3,49]; Co-doping was also used to enhance the electrocatalytic performance of $FeSe_2$ [49]. However, potential performance of $FeSe_2$ has not been fully realized and the challenges associated with further improvement of the electrochemical activity can be addressed by introducing a conductive MWCNT support. Therefore, we propose that the incorporation of modified MWCNT can be advantageous simultaneously for improving the morphology of $FeSe_2$ and the charge transfer. To the best of our knowledge, the synergistic effect between $FeSe_2$ and MWCNT has not been reported yet.

Herein, we demonstrate a simple one-pot hydrothermal synthesis protocol for fabricating MWCNT/$FeSe_2$ composite. Growth and morphology of $FeSe_2$ are significantly affected by functionalized MWCNT resulting in reduced agglomeration. This study highlights the synergistic effect between MWCNT and $FeSe_2$ for HET and HER. While $FeSe_2$ is an HER catalyst with sluggish HET kinetics in response to the $[Ru(NH_3)_6]^{3+/2+}$ redox probe, MWCNT/$FeSe_2$ demonstrates an improved electrochemical activity. Such a conductive MWCNT network supporting $FeSe_2$ is beneficial for sensing and electrocatalytic applications.

2. Experimental section

2.1. Chemicals

The following chemicals were used in this study: iron (III) chloride hexahydrate (Sigma-Aldrich, ≥97%), hydrazine monohydrate 64–65% (Sigma-Aldrich, 98%), selenium (Sigma, 99.999%, −100 mesh), multi-walled carbon nanotubes (Nanostructured & Amorphous Materials Inc., OD: 50–100 nm, ID: 5–10 nm, length: 5–10 μm, 95% purity), nitric acid (Sigma-Aldrich, 70%), sulfuric acid (Sigma-Aldrich, 96%), potassium chloride (Sigma-Aldrich analytical grade), hexamine ruthenium (III) chloride (Sigma-Aldrich 98%), nafion® 117 solution (Sigma-Aldrich), and 20 wt% platinum on carbon (Fuel Cell Store).

2.2. Synthesis of MWCNT/$FeSe_2$ composite

$FeSe_2$ decorated multi-walled carbon nanotube composite was synthesized by a one-pot hydrothermal process. Prior to the hydrothermal synthesis, functionalization of pristine MWCNT was performed in a mixture of concentrated nitric acid and concentrated sulfuric acid at 60 °C for 2 h under continuous ultrasonication [50]. Functionalized MWCNT was washed with DI water and ethanol followed by filtration and vacuum-drying at 70 °C overnight. 17 mg of thus-prepared functionalized MWCNT was ultrasonically dispersed in 25 mL of DI water and then 1 mmol of $FeCl_3 \cdot 6H_2O$ was dissolved in the solution. 2 mmol of Se was dissolved in 8 mL of hydrazine monohydrate at room temperature and subsequently mixed with the $FeCl_3$ containing solution. Hydrazine also serves as the reducing agent [51]. The mixture was transferred into a 45 mL Teflon stainless-steel autoclave and it was kept at 180 °C for 10 h in an electric oven. The product was collected via filtration and washed several times with DI water and ethanol followed by vacuum drying at 80 °C overnight to obtain $FeSe_2$ decorated MWCNT (MWCNT/$FeSe_2$). Plain $FeSe_2$ was obtained using the same hydrothermal synthesis without the addition of functionalized MWCNT.

2.3. Characterization

X-ray diffraction (XRD) patterns were obtained using a Rigaku Miniflex-II with Cu Kα (λ = 1.5406 Å) radiation at 30 kV and 15 mA. Morphological characterization was performed with a JEOL 2010 transmission electron microscope (TEM). X-ray photoelectron spectroscopy (XPS) analysis was conducted with a Thermo Fisher ESCALAB 250Xi using the Al Kα X-ray source (1486.6 eV). The XPS spectra were calibrated with adventitious carbon peak at 284.8 eV.

2.4. Electrochemical measurements

All electrochemical measurements were conducted in a three-electrode cell configuration with Pt coil and Ag/AgCl (4 M KCl) as the counter and the reference electrodes, respectively. To fabricate the working electrode, 5 mg of MWCNT/$FeSe_2$ was dispersed in 1 mL of ethanol-nafion solution (950 μL absolute ethanol: 50 μL nafion solution) and ultrasonicated for 30 min to achieve a homogenous ink. The glassy carbon electrode (GCE) surface was polished using three alumina suspensions decreasing in particle size (5, 3, and 0.05 μm; Allied High Tech Products). The polished surface was washed with DI water and air-dried before 5 μL of the catalyst ink was drop-casted on it (surface area: 0.1976 cm^2). Working electrodes with plain $FeSe_2$, pristine MWCNT, and

platinum on carbon (Pt/C) [20 wt%] were similarly prepared. The mass loading of the catalyst was ~0.126 mg/cm^2.

Both HET and HER activities were measured using a CHI 760C electrochemical station. The HET kinetics was studied using 5 mM hexaaminеruthenium (III) chloride and typically in 0.1 M KCl unless mentioned otherwise. The solution was bubbled with nitrogen for 15 min prior to each electrochemical measurement. Electrode characteristics were evaluated using the cyclic voltammograms (CV) obtained at various scan rates. For HER, 0.5 M H_2SO_4 was used as the electrolyte. Linear sweep voltammetry (LSV) was performed at 5 mV/s. The working electrode potentials vs. Ag/AgCl were converted into the reversible hydrogen electrode (RHE) potential utilizing the Nernst equation: $E_{RHE} = E_{Ag/AgCl} + 0.059\,pH + E^0_{Ag/AgCl}$ without taking iR compensation into account. Electrochemical impedance spectroscopy (EIS) measurements were conducted in 0.5 M H_2SO_4 from 10^5 Hz to 0.1 Hz at an overpotential of 0.295 V vs. RHE and 5 mV AC amplitude.

3. Results and discussion

3.1. Characterization of the catalysts

Fig. 1 shows the XRD patterns of $FeSe_2$ and MWCNT/$FeSe_2$. The crystallographic phase of $FeSe_2$ corresponds to an orthorhombic crystal (JCPDS No. 79-1892) of a *Pnnm* space group with a = 4.803 Å, b = 5.751 Å, and c = 3.566 Å, respectively. The diffraction peak associated with the (002) plane of MWCNT [52] at 2θ = 26.3° is weak due to the overwhelming signal of $FeSe_2$ in the composite. Fig. 2 presents the TEM images of MWCNT/$FeSe_2$ composite and plain $FeSe_2$. It had been reported that hydrophilic groups of functionalized MWCNT work as anchors [52] improving adhesion of other TMDC onto MWCNT, which we observe here for $FeSe_2$ in Fig. 2a and b. Moreover, $FeSe_2$ alone without functionalized MWCNT is aggregated into noticeably larger particles, as shown in Fig. 2c. The dispersion of $FeSe_2$ suggests that functionalized MWCNT not only acts as a support for $FeSe_2$ but also regulates its growth. A high resolution TEM image in Fig. 2d reveals that $FeSe_2$ is crystalline and its lattice spacing of ~0.37 nm corresponds to the (110) plane of $FeSe_2$.

The XPS analysis presented in Fig. 3 was carried out to evaluate the chemical states of elements in MWCNT/$FeSe_2$. The survey spectrum of MWCNT/$FeSe_2$ (Fig. 3a) indicates the contribution of Fe, Se, C, and O in the composite. The peaks at 707.9 and 711.1 eV correspond to the Fe $2p_{3/2}$ signal (Fig. 3b) [49,53]. The minor peak at 707.9 eV indicates the Fe-Fe interaction, while the peak at 711.06 eV is attributed to Fe^{2+} bonded with Se ions [53,54]. The signals at 719.76 and 725 eV likely arise from Fe $2p_{1/2}$ [55]. The fitted XPS spectrum in Fig. 3c shows the Se 3d signal at 55.3 eV indicating the formation of $FeSe_2$ [53,56]. The minor peak at 58.7 eV suggests that surface oxidation of selenium species also takes place [55,57]. The intense peak in the C 1s region of the spectrum in Fig. 3d is assigned to the sp^2 hybridized carbon, while other peaks with reduced intensities are associated with C–O, C═O, and O–C═O groups [58]. These XPS assignments and intensities are consistent with other reports on the chemical states of similar species.

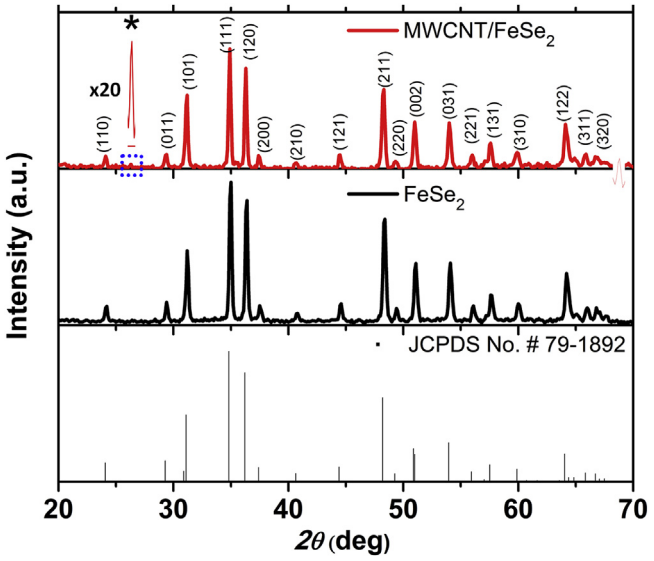

Fig. 1. XRD patterns of $FeSe_2$ and MWCNT/$FeSe_2$. The (002) MWCNT peak indicated by * is zoomed showing the characteristic peak at 2θ = 26.31°.

3.2. Heterogeneous electron transfer (HET)

The HET kinetics at an electrode provide the necessary assessment of its potential applications in electrochemical sensing, energy storage and conversion, etc. [25,32,37,39] We studied the kinetics at the electrode-electrolyte interface with $[Ru(NH_3)_6]^{3+/2+}$ redox probe using the CV measurements at different scan rates for all three electrode materials: MWCNT, $FeSe_2$, and MWCNT/$FeSe_2$. $[Ru(NH_3)_6]^{3+/2+}$ is known to be practically unaffected by the surface modifications of the electrodes [35,38,59,60]; its outer sphere charge transfer is almost independent of the specifics of the surface sites. Therefore, changes in the electrode characteristics should correspond primarily to the materials electronic properties [38,59,60]. The CV measurements with MWCNT, $FeSe_2$, and MWCNT/$FeSe_2$ electrodes are presented in Fig. 4a–c, where the well-defined peaks in the anodic and cathodic scans for $[Ru(NH_3)_6]^{3+/2+}$ are clearly observed. The redox peaks with MWCNT/$FeSe_2$ are sharper than those of either MWCNT or $FeSe_2$ alone. For all three choices of the electrode, the current density in CV increases linearly with the (scan rate)^{½}, as expected for diffusion controlled reactions (Fig.SI-2), but the separation potential between the cathodic and anodic peaks (ΔE_p) exceeds 59/n mV (Table SI-1) [61,62] expected for fully reversible reaction and increases with the scan rate. The peak separation potentials in the range from ~62/n mV to 1000/n mV correspond to the case of a quasi-reversible electrode [23,29], *i.e.* when the CV response is limited by the rates of the electron transfer reaction rather than solely by diffusion [61]. The peak current ratio is also dependent on the scan rate, as shown in Fig. 4d. It is less than unity in all the presented there cases but is more pronounced for the composite. At least in part, the effect is due to the nonzero surface charge as is illustrated in Fig. SI-1. The surface charge of $FeSe_2$ at neutral pH is negative (pI is 1.4–1.8) [63–65] and so is that of activated MWCNT (due to the introduced carboxyl groups with pKa~3 or less) [66,67]. Thus the negatively charged ions (like $[Fe(CN)_6]^{3-/4-}$) are effectively repelled at low electrolyte concentration but the positively charged $Ru(NH_3)_6]^{3+/2+}$ are attracted to the surface. Moreover, because $Ru(NH_3)_6]^{3+}$ is more charged than $Ru(NH_3)_6]^{2+}$, the concentration of the former near the surface (i.e. after anodic part of the cycle) is higher and results in a higher cathodic signal afterwards. Due to that, the ratio in Fig. 4d is below unity for all cases but it is more pronounced for MWCNT/FeS_2 composite, maybe due to a synergistic effect.

Both, the peak current ratio less than unity and the peak separation potential, suggest an overall quasi-reversible electrochemical process at the electrode-electrolyte interface [61,68], which can be formalized by relating the heterogeneous electron transfer rate constant (k^0) to the mass transport coefficient $[m_T =$

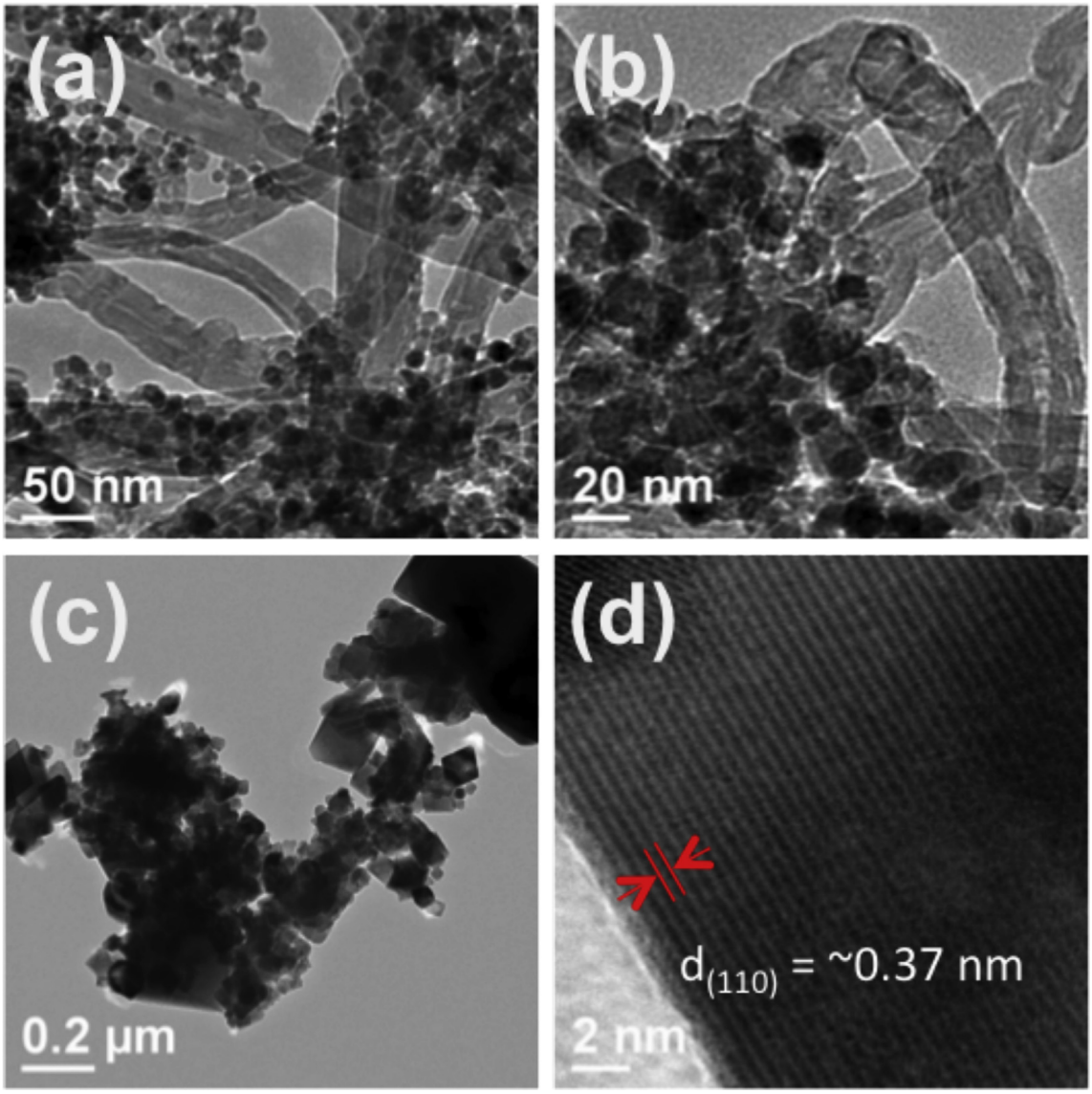

Fig. 2. TEM images of MWCNT/$FeSe_2$ (**a** & **b**) and $FeSe_2$ alone (**c** &**d**).

$\left(\frac{FDv}{RT}\right)^{1/2}\Big]$. The values of k^0 can be calculated as a slope from the plots of the dimensionless charge transfer parameter (ψ) *vs.* (scan rate)$^{-1/2}$ using the Nicholson formula [23,69]:

$$\psi = k^0\left(\frac{\pi nF\upsilon D}{RT}\right)^{-1/2}\left(\frac{D_R}{D_O}\right)^{-\alpha/2} \quad (1)$$

where, n, υ, α, F, D, R, and T are the number of electrons transferred, the scan rate, the transfer coefficient ($\alpha = 0.5$), the Faraday constant, the diffusion constant, the gas constant, and the absolute temperature, respectively. ψ can be obtained from the peak separation potential via an approximation valid for $\Delta E_p < 220$ mV [23,62,69,70]:

$$\ln(\psi) = 3.69 - 1.16ln(\Delta E_p - 59) \quad (2)$$

The diffusion constants for the reduced (D_R) and oxidized species (D_O) for the $[Ru(NH_3)_6]^{3+/2+}$ redox probe were taken to be equal and calculated using the Randles-Ševćik equation [71], $D = D_R = D_O = 3.19 \times 10^{-6}$ cm^2/s. The quasi-reversible behavior [62] can be illustrated using the Matsuda-Ayabe parameter, $\xi = \frac{k^0}{m_T}$ [66]. The value of ξ at different scan rates (Fig. SI-3) reveals the competitive behavior: ξ is on the order of unity and decreases with the scan rate but for the MWCNT/$FeSe_2$ composite, it is the largest. It confirms that all of them are quasi-reversible but MWCNT/$FeSe_2$ possesses a greater HET activity than that of MWCNT and $FeSe_2$.

The HET rate constants for pristine MWCNT, $FeSe_2$ and the MWCNT/$FeSe_2$ composite obtained from the ψ vs. (scan rate)$^{-1/2}$ plots are 3.4×10^{-3}, 1.7×10^{-3}, and 5.4×10^{-3} cm/s, respectively. The highest value of k^0 for the composite (58% higher than for plain $FeSe_2$) is directly related to its lowest peak separation potential, as shown in Fig. 5a and b. We speculate that the improved HET performance of the MWCNT/$FeSe_2$ composite is due to the synergistic effect, where conductive MWCNT supports $FeSe_2$ nanoparticles and increases their active surface area [33,40]. Thus, the overall HET kinetics is quasi-reversible for all electrodes and changes in the following order: $\Delta E_{p|MWCNT/FeSe2} < \Delta E_{p|MWCNT} < \Delta E_{p|FeSe2}$ corresponding to $k^0_{FeSe2} < k^0_{MWCNT} < k^0_{MWCNT/FeSe2}$.

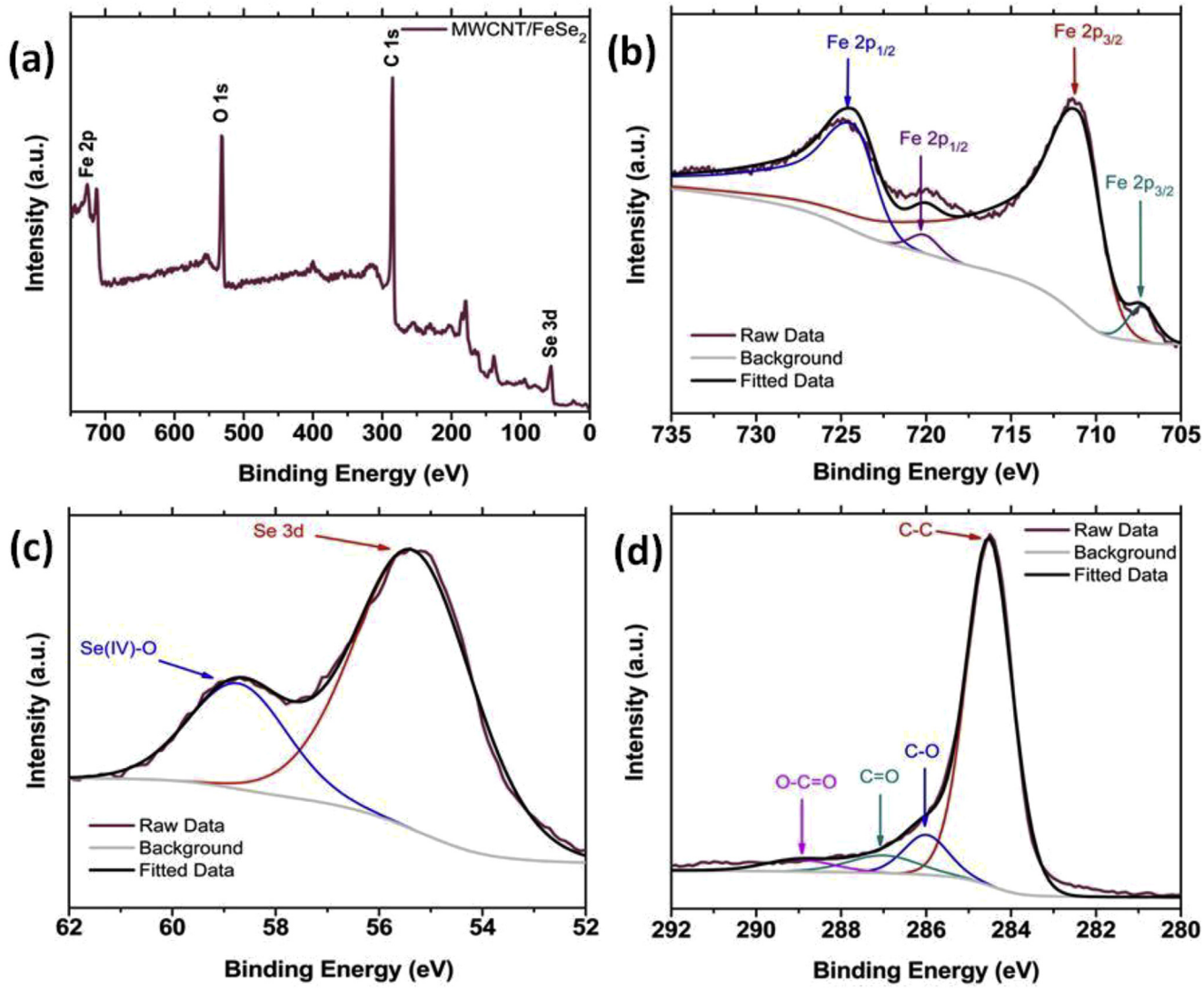

Fig. 3. XPS survey spectrum of MWCNT/$FeSe_2$ (**a**), and its zoomed parts: Fe 2p spectrum (**b**), Se 3d spectrum (**c**), and C 1s spectrum (**d**).

3.3. *Electrochemical hydrogen evolution reaction (HER)*

Electrocatalytic measurements of HER were carried out in 0.5 M H_2SO_4 using a standard three-electrode set-up. A suitable HER catalyst should demonstrate a high current density at a lower overpotential [16]. Therefore, polarization curves were generated for pristine MWCNT, $FeSe_2$, MWCNT/$FeSe_2$, and commercial Pt/C, (Fig. 6a). Pt/C electrocatalyst demonstrates the lowest onset potential and the highest current density at a smaller overpotential. In contrast to Pt/C, MWCNT electrode shows negligible catalytic activity, consistent with other reports [72]. However, $FeSe_2$ and MWCNT/$FeSe_2$ exhibit significant catalytic HER activities implying that $FeSe_2$ serves as the core HER catalyst in both cases. Again, the overpotential required to deliver 10 mA/cm^2 is lower for the composite. It also demonstrates a correspondingly smaller onset potential (Fig. SI-4). Further insight into the improved catalytic activity of MWCNT/$FeSe_2$ can be obtained from the Tafel plots presented in Fig. 6b. Tafel slope signifies the additional voltage required to generate the current density of an order of magnitude [73,74]. The linear portions of the Tafel plots were fit with the Tafel equation: $\eta = b\ log\ |j| + a$, where η, b, and j are overpotential, Tafel slope, and current density, respectively. Electrocatalytic hydrogen evolution kinetics are usually explained via either the Volmer-Heyrovsky or the Volmer-Tafel pathways [21,75]. As shown in Fig. 6b, Pt/C, with a Tafel slope of 28 mV/dec, follows what is expected in the Volmer-Tafel reaction pathway, where chemical desorption of hydrogen atom is the rate-limiting step at low overpotentials [76,77]. Although the Tafel slope of 70 mV/dec for MWCNT/$FeSe_2$ is greater than that of Pt/C but it is 11% smaller than for $FeSe_2$ (78 mV/dec). Such relatively high Tafel slopes suggest that the HER process for both of them is more likely to proceed via the Volmer-Heyrovsky reaction pathway [3], where hydronium ions are reduced to hydrogen atoms on the active sites leading to hydrogen generation and its subsequent desorption. However, the actual assessment of the Tafel slope still remains inconclusive owing to the complexities of multiple reaction steps during the HER [21,75]. Nonetheless, a better HER activity of the MWCNT/$FeSe_2$ composite over $FeSe_2$ can be credited to the synergistic effect [78,79] of the improved conductivity due MWCNT and a greater number of active sites in smaller size of $FeSe_2$.

Enhancement in the HER activity of MWCNT/$FeSe_2$ was further confirmed by the differences in relative electrochemically active surface area (ECSA), which can be also evaluated from the CVs. The ECSA can be related to the electrochemical double-layer

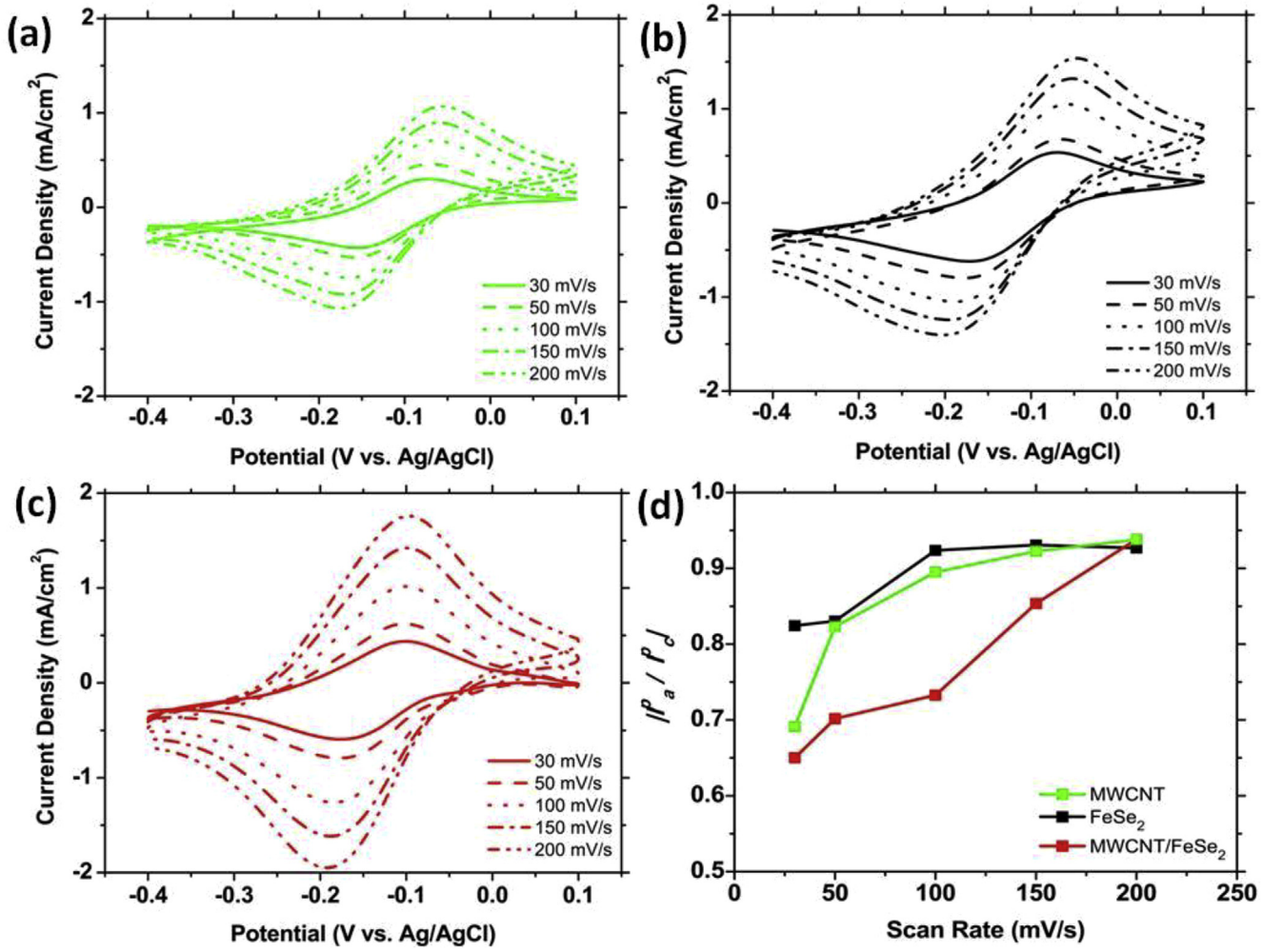

Fig. 4. Cyclic voltammograms for $[Ru(NH_3)_6]^{3+/2+}$ redox probe with MWCNT (**a**), $FeSe_2$ (**b**), and MWCNT/$FeSe_2$ (**c**) electrodes at various scan rates. Profiles of the anodic/cathodic peak current ratio as a function of the scan rate (**d**).

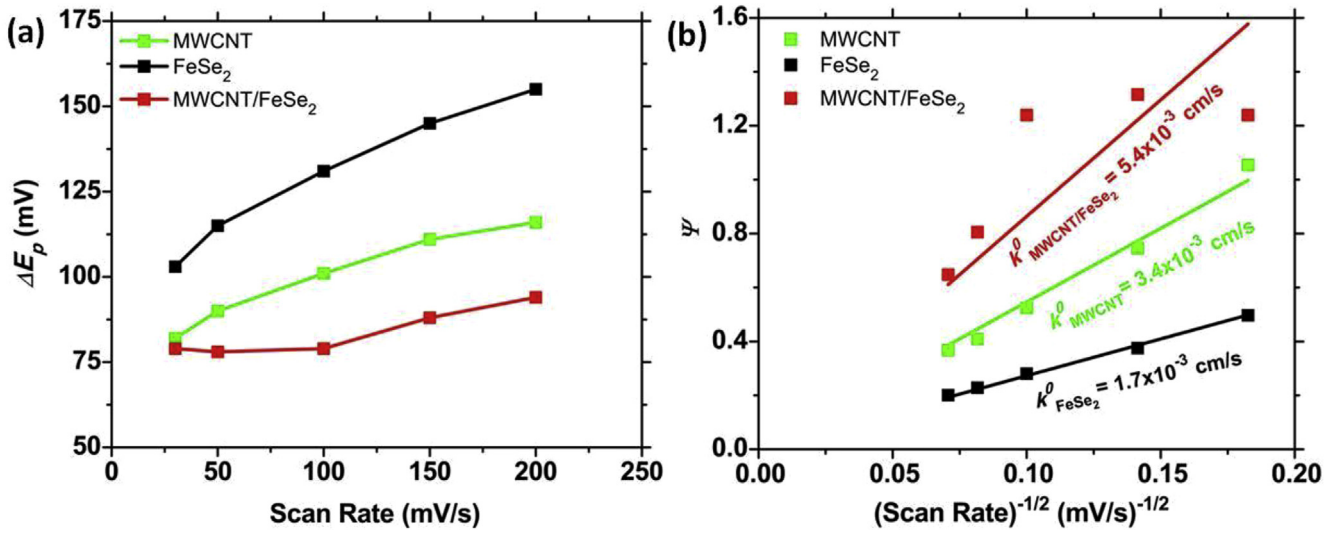

Fig. 5. Plots of the peak separation potential (**a**) and the evaluation of the electron transfer rate constant (**b**) for MWCNT, $FeSe_2$, and MWCNT/$FeSe_2$.

capacitance (C_{dl}) measured within the non-Faradaic region [80]. Representative CVs of $FeSe_2$ and MWCNT/$FeSe_2$ generated at various scan rates are presented in Fig. SI-5. The C_{dl} values were calculated from the plot of $\Delta j = (j_a - j_c)/2$ at 0.445 V vs. RHE against

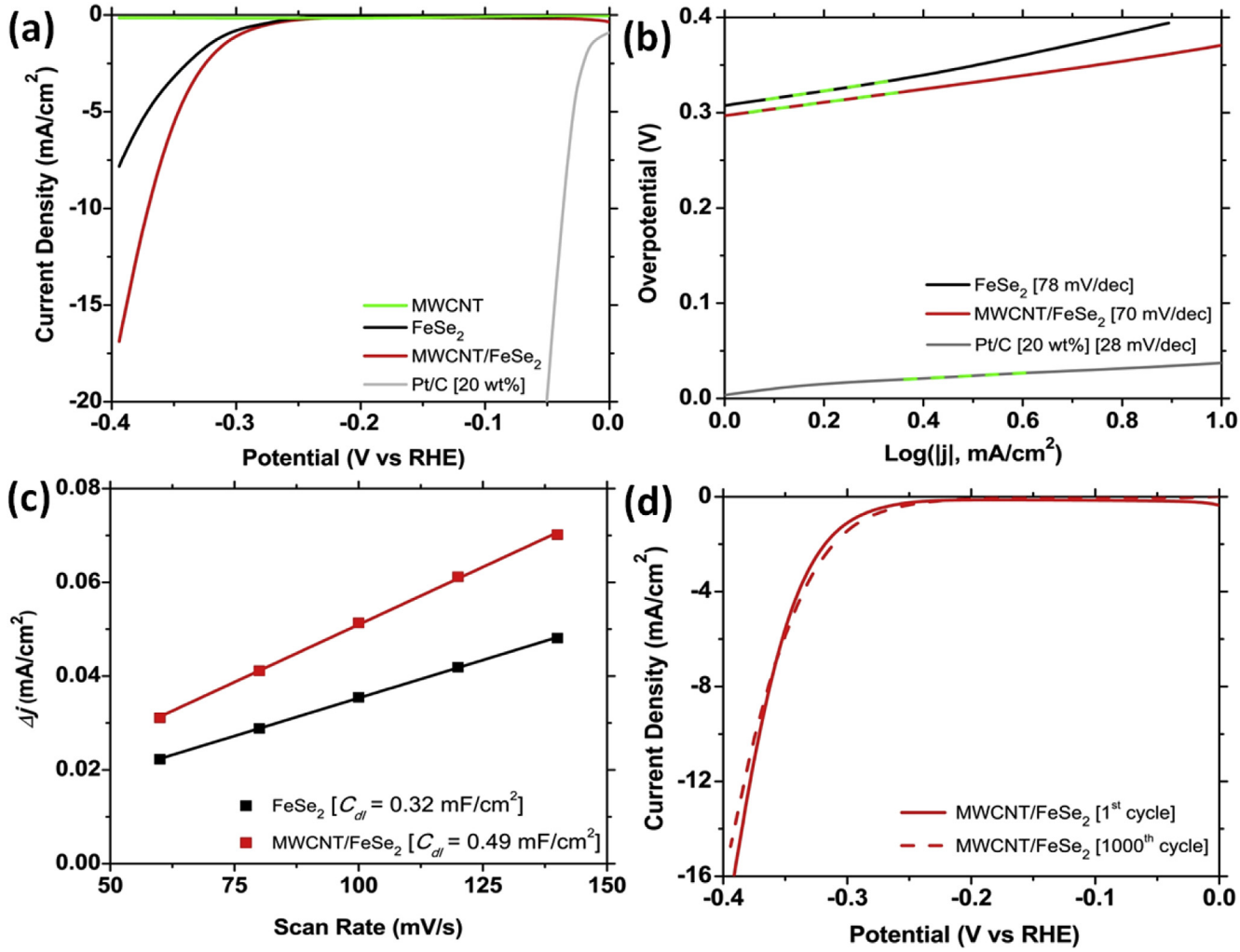

Fig. 6. LSV polarization curves (**a**), Tafel plots (**b**), plots of the current density difference [$\Delta j = (j_a - j_c)/2$] at 0.445 V vs. RHE as a function of the scan rate (**c**), and the stability analysis illustrating the 1st and the 1000th LSV polarization curves of MWCNT/$FeSe_2$ (**d**). All plots were obtained in 0.5 M H_2SO_4.

the scan rates, as presented in Fig. 6c. An apparent higher value of C_{dl} for the MWCNT/$FeSe_2$ composite (0.491 mF/cm^2) than that of $FeSe_2$ (0.323 mF/cm^2) suggests the presence of a higher ECSA for the composite. Therefore, incorporation of $FeSe_2$ with functionalized MWCNT is an effective way to increase the number of active sites and thus improve HER activity. Further insights into the electrode kinetics and the charge transfer were obtained from the impedance spectroscopy. Nyquist plots (Fig. SI-6) show that MWCNT/$FeSe_2$ possesses a substantially lower charge transfer resistance (R_{ct}) of 121 Ω than that of $FeSe_2$ (436 Ω). The error in the simulated parameters is below 3%. A smaller R_{ct} for the composite reflects a faster Faradaic process towards hydrogen generation at the electrode-electrolyte interface. The corresponding Bode plots (Fig. SI-6) can be explained using a one-time-constant process with the charge transfer times (τ) evaluated according to the equation: $\tau = \frac{1}{\omega_p}$, where ω_p is the angular frequency at the peak in the -Phase vs. $log(\omega)$ plot [13]. The MWCNT/$FeSe_2$ composite has a smaller charge transfer time (1.44 ms) than that of $FeSe_2$ (2.22 ms). The catalytic stability is another important parameter for the HER activity. Comparison of the linear sweep voltammograms of MWCNT/$FeSe_2$ for the 1st and 1000th cycles shows that MWCNT/$FeSe_2$ composite is a fairly stable electrocatalyst for hydrogen generation (Fig. 6d). The gradual decrease in the catalytic activity might be associated with the corrosion of the catalyst in the acidic media.

4. Conclusions

In summary, the MWCNT/$FeSe_2$ composite fabricated using the one-pot hydrothermal process shows a synergistic improvement in the heterogeneous electron transfer and the electrocatalytic hydrogen evolution reaction. Significantly improved HET rate constant for $[Ru(NH_3)_6]^{3+/2+}$ redox probe in 0.1 M KCl (to 5.4×10^{-3} cm/s or by 58% compared to plain $FeSe_2$) and a smaller Tafel slope (70 mV/dec) during hydrogen evolution for the composite highlight its superiority over MWCNT and $FeSe_2$ alone. The synergistic enhancement arises from the increased surface area of smaller $FeSe_2$ particles and the presence of conductive MWCNT support. The promising approach may be further improved by doping and better controlled morphological alterations of the catalysts, which can be applied in electrochemical sensing and electrocatalytic hydrogen evolution.

Author contributions

H. Luo and S.N. Smirnov supervised this project. S. Sarker and P. Chaturvedi conceived the research and prepared the manuscript with contribution from other co-authors. The final version of the

manuscript was approved by all authors.

Acknowledgements

Dr. Luo thanks the support from New Mexico EPSCoR (NSF-1301346) and the USDA National Institute of Food and Agriculture, HSI Collaboration: Integrating Food Science/Engineering and Education Network (IFSEEN, award number: 2015-38422-24059). This work made use of the Keck-II facility of Northwestern University's NUANCE Center, which has received support from the Soft and Hybrid Nanotechnology Experimental (SHyNE) Resource (NSF ECCS-1542205); the MRSEC program (NSF DMR-1121262) at the Materials Research Center; the International Institute for Nanotechnology (IIN); the Keck Foundation; and the State of Illinois, through the IIN. We also acknowledge the TEM facility at the Los Alamos National Laboratory, NM.

Appendix A. Supplementary data

Supplementary data related to this article can be found at https://doi.org/10.1016/j.electacta.2018.03.064.

References

[1] S. Wu, Z. Zeng, Q. He, Z. Wang, S.J. Wang, Y. Du, Z. Yin, X. Sun, W. Chen, H. Zhang, Electrochemically reduced single-layer MoS_2 nanosheets: characterization, properties, and sensing applications, Small 8 (2012) 2264–2270.
[2] Z. He, W. Que, Molybdenum disulfide nanomaterials: structures, properties, synthesis and recent progress on hydrogen evolution reaction, Appl. Mater. Today 3 (2016) 23–56.
[3] J. Theerthagiri, R. Sudha, K. Premnath, P. Arunachalam, J. Madhavan, A.M. Al-Mayouf, Growth of iron diselenide nanorods on graphene oxide nanosheets as advanced electrocatalyst for hydrogen evolution reaction, Int. J. Hydrogen Energy 42 (2017) 13020–13030.
[4] R. Gao, H. Zhang, D. Yan, Iron diselenide nanoplatelets: stable and efficient water-electrolysis catalysts, Nanomater. Energy 31 (2017) 90–95.
[5] H. Zhou, F. Yu, Y. Huang, J. Sun, Z. Zhu, R.J. Nielsen, R. He, J. Bao, W.A. Goddard III, S. Chen, Z. Ren, Efficient hydrogen evolution by ternary molybdenum sulfoselenide particles on self-standing porous nickel diselenide foam, Nat. Commun. 7 (2016) 12765–12771.
[6] H.I. Karunadasa, E. Montalvo, Y. Sun, M. Majda, J.R. Long, C.J. Chang, A molecular MoS_2 edge site mimic for catalytic hydrogen generation, Science 335 (2012) 698–702.
[7] L. Dai, Y. Xue, L. Qu, H.-J. Choi, J.-B. Baek, Metal-free catalysts for oxygen reduction reaction, Chem. Rev. 115 (2015) 4823–4892.
[8] U. Martinez, J.H. Dumont, E.F. Holby, K. Artyushkova, G.M. Purdy, A. Singh, N.H. Mack, P. Atanassov, D.A. Cullen, K.L. More, M. Chhowalla, P. Zelenay, A.M. Dattelbaum, A.D. Mohite, G. Gupta, Critical role of intercalated water for electrocatalytically active nitrogen-doped graphitic systems, Sci. Adv. 2 (2016) e1501178–e1501178.
[9] J. He, P. Li, W. Lv, K. Wen, Y. Chen, W. Zhang, Y. Li, W. Qin, W. He, Three-dimensional hierarchically structured aerogels constructed with layered MoS_2/graphene nanosheets as free-standing anodes for high-performance lithium ion batteries, Electrochim. Acta 215 (2016) 12–18.
[10] K. Zhang, Z. Hu, X. Liu, Z. Tao, J. Chen, $FeSe_2$ microspheres as a high-performance anode material for Na-ion batteries, Adv. Mater. 27 (2015) 3305–3309.
[11] W. Yin, L. Yan, J. Yu, G. Tian, L. Zhou, X. Zheng, X. Zhang, High-throughput synthesis of single-layer MoS_2 nanosheets as a near-infrared photothermal-triggered drug delivery for effective cancer therapy, ACS Nano 8 (2014) 6922–6933.
[12] J. Deng, H. Li, S. Wang, D. Ding, M. Chen, C. Liu, Z. Tian, K.S. Novoselov, C. Ma, D. Deng, X. Bao, Multiscale structural and electronic control of molybdenum disulfide foam for highly efficient hydrogen production, Nat. Commun. 8 (2017) 14430–14437.
[13] W.-H. Hu, X. Shang, J. Xue, B. Dong, J.-Q. Chi, G.-Q. Han, Y.-R. Liu, X. Li, K.-L. Yan, Y.-M. Chai, C.-G. Liu, Activating MoS_2/CNs by tuning (001) plane as efficient electrocatalysts for hydrogen evolution reaction, Int. J. Hydrogen Energy 42 (2017) 2088–2095.
[14] Z. Chen, K. Leng, X. Zhao, S. Malkhandi, W. Tang, B. Tian, L. Dong, L. Zheng, M. Lin, B.S. Yeo, K.P. Loh, Interface confined hydrogen evolution reaction in zero valent metal nanoparticles-intercalated molybdenum disulfide, Nat. Commun. 8 (2017) 14548–14556.
[15] D. Voiry, R. Fullon, J. Yang, C. de Carvalho Castro e Silva, R. Kappera, I. Bozkurt, D. Kaplan, M.J. Lagos, P.E. Batson, G. Gupta, A.D. Mohite, L. Dong, D. Er, V.B. Shenoy, T. Asefa, M. Chhowalla, The role of electronic coupling between substrate and 2D MoS_2 nanosheets in electrocatalytic production of hydrogen, Nat. Mater. 15 (2016) 1003–1009.
[16] H. Tang, K. Dou, C.-C. Kaun, Q. Kuang, S. Yang, $MoSe_2$ nanosheets and their graphene hybrids: synthesis, characterization and hydrogen evolution reaction studies, J. Mater. Chem. A 2 (2014) 360–364.
[17] P.K. Rastogi, S. Sarkar, D. Mandler, Ionic strength induced electrodeposition of two-dimensional layered MoS_2 nanosheets, Appl. Mater. Today 8 (2017) 44–53.
[18] H. He, J. Lin, W. Fu, X. Wang, H. Wang, Q. Zeng, Q. Gu, Y. Li, C. Yan, B.K. Tay, C. Xue, X. Hu, S.T. Pantelides, W. Zhou, Z. Liu, MoS_2/TiO_2 edge-on heterostructure for efficient photocatalytic hydrogen evolution, Adv. Energy Mater. 6 (2016) 1–7.
[19] T.L. Levalley, A.R. Richard, M. Fan, The progress in water gas shift and steam reforming hydrogen production technologies - a review, Int. J. Hydrogen Energy 39 (2014) 16983–17000.
[20] I. Roger, M.A. Shipman, M.D. Symes, Earth-abundant catalysts for electrochemical and photoelectrochemical water splitting, Nat. Rev. Chem. 1 (3) (2017) 41570–41582.
[21] Y. Zheng, Y. Jiao, M. Jaroniec, S.Z. Qiao, Advancing the electrochemistry of the hydrogen- Evolution reaction through combining experiment, Angew. Chem. Int. Ed. 54 (2015) 52–65.
[22] Z.W. Seh, J. Kibsgaard, C.F. Dickens, I. Chorkendorff, J.K. Nørskov, T.F. Jaramillo, Combining theory and experiment in electrocatalysis: insights into materials design, Science 355 (2017) 146–157.
[23] A.J. Bard, L.R. Faulkner, Electrochemical Methods: Fundamentals and Applications, second ed., Willey, New York, 2001.
[24] S. Chen, Y. Liu, J. Chen, Heterogeneous electron transfer at nanoscopic electrodes: importance of electronic structures and electric double layers, Chem. Soc. Rev. 43 (2014) 5372–5386.
[25] X. Mao, F. Guo, E.H. Yan, G.C. Rutledge, T. Alan Hatton, Remarkably high heterogeneous electron transfer activity of carbon-nanotube-supported reduced graphene oxide, Chem. Mater. 28 (2016) 7422–7432.
[26] R.L. McCreery, Advanced carbon electrode materials for molecular electrochemistry, Chem. Rev. 108 (2008) 2646–2687.
[27] T.J. Davies, M.E. Hyde, R.G. Compton, Nanotech arrays reveal insight into graphite electrochemistry, Angew. Chem. Int. Ed. 44 (2005) 5121–5126.
[28] I. Streeter, G.G. Wildgoose, L. Shao, R.G. Compton, Cyclic voltammetry on electrode surfaces covered with porous layers: an analysis of electron transfer kinetics at single-walled carbon nanotube modified electrodes, Sensors Actuators B Chem. 133 (2008) 462–466.
[29] M. Velicky, D.F. Bradley, A.J. Cooper, E.W. Hill, I.A. Kinloch, A. Mishchenko, K.S. Novoselov, H. V Patten, P.S. Toth, A.T. Valota, S.D. Worrall, R.A.W. Dryfe, Electron Transfer kinetics on mono- and multilayer graphene, ACS Nano 8 (2014) 10089–10100.
[30] D.A.C. Brownson, D.K. Kampouris, C.E. Banks, Graphene electrochemistry: fundamental concepts through to prominent applications, Chem. Soc. Rev. 41 (2012) 6944–6976.
[31] P.A. Henry, A.S. Raut, S.M. Ubnoske, C.B. Parker, J.T. Glass, Enhanced electron transfer kinetics through hybrid graphene-carbon nanotube films, Electrochem. Commun. 48 (2014) 103–106.
[32] Y. Yu, Z. Chen, S. He, B. Zhang, X. Li, M. Yao, Direct electron transfer of glucose oxidase and biosensing for glucose based on PDDA-capped gold nanoparticle modified graphene/multi-walled carbon nanotubes electrode, Biosens. Bioelectron. 52 (2014) 147–152.
[33] J. Friedl, U. Stimming, Determining electron transfer kinetics at porous electrodes, Electrochim. Acta 227 (2017) 235–245.
[34] A.G. Güell, N. Ebejer, M.E. Snowden, J. V Macpherson, R. Patrick, Structural correlations in heterogeneous electron transfer at monolayer and multilayer graphene electrodes, J. Am. Chem. Soc. 134 (2012) 7258–7261.
[35] J. Kim, A.J. Bard, Electrodeposition of single nanometer-size Pt nanoparticles at a tunneling ultramicroelectrode and determination of fast heterogeneous kinetics for $[Ru(NH_3)_6]^{3+}$ reduction, J. Am. Chem. Soc. 138 (2016) 975–979.
[36] D.A.C. Brownson, L.J. Munro, D.K. Kampouris, C.E. Banks, Electrochemistry of graphene: not such a beneficial electrode material? RSC Adv. 1 (2011) 978–988.
[37] A.Y.S. Eng, A. Ambrosi, Z. Sofer, P. Šimek, M. Pumera, Electrochemistry of transition metal dichalcogenides: strong dependence on the metal-to-chalcogen composition and exfoliation method, ACS Nano 8 (2014) 12185–12198.
[38] M. Velický, M.A. Bissett, C.R. Woods, P.S. Toth, T. Georgiou, I.A. Kinloch, K.S. Novoselov, R.A.W. Dryfe, Photoelectrochemistry of pristine mono- and few-layer MoS_2, Nano Lett. 16 (2016) 2023–2032.
[39] X. Chia, A. Ambrosi, Z. Sofer, J. Luxa, M. Pumera, Catalytic and charge transfer properties of transition metal dichalcogenides arising from electrochemical pretreatment, ACS Nano 9 (2015) 5164–5179.
[40] S.M. Tan, A. Ambrosi, Z. Sofer, S. Huber, D. Sedmidubsky, M. Pumera, Pristine basal- and edge-plane-oriented molybdenite MoS_2 exhibiting highly anisotropic properties, Chem. Eur J. 21 (2015) 7170–7178.
[41] D. Nkosi, J. Pillay, K.I. Ozoemena, K. Nouneh, M. Oyama, Heterogeneous electron transfer kinetics and electrocatalytic behaviour of mixed self-assembled ferrocenes and SWCNT layers, Phys. Chem. Chem. Phys. 12 (2010) 604–613.
[42] D. Ragupathy, A.I. Gopalan, K.P. Lee, Synergistic contributions of multiwall carbon nanotubes and gold nanoparticles in a chitosan-ionic liquid matrix towards improved performance for a glucose sensor, Electrochem. Commun. 11 (2009) 397–401.

[43] J. Li, J.D. Qiu, J.J. Xu, H.Y. Chen, X.H. Xia, The synergistic effect of prussian-blue-grafted carbon nanotube/poly(4-vinylpyridine) composites for amperometric sensing, Adv. Funct. Mater. 17 (2007) 1574–1580.
[44] W. Wang, X. Pan, W. Liu, B. Zhang, H. Chen, X. Fang, J. Yao, S. Dai, $FeSe_2$ films with controllable morphologies as efficient counter electrodes for dye-sensitized solar cells, Chem. Commun. (J. Chem. Soc. Sect. D) 50 (2014) 2618–2620.
[45] C. Wombwell, C.A. Caputo, E. Reisner, [NiFeSe]-Hydrogenase chemistry, Acc. Chem. Res. 48 (2015) 2858–2865.
[46] D. Kong, J.J. Cha, H. Wang, H.R. Lee, Y. Cui, First-row transition metal dichalcogenide catalysts for hydrogen evolution reaction, Energy Environ. Sci. 6 (2013) 3553–3558.
[47] T. Mahalingam, S. Thanikaikarasan, R. Chandramohan, M. Raja, C. Sanjeeviraja, J.H. Kim, Y.D. Kim, Effects of bath temperature in electrodeposited $FeSe_2$ thin films, Mater. Chem. Phys. 106 (2007) 369–374.
[48] B. Ouertani, J. Ouerfelli, M. Saadoun, M. Zribi, M.B. Rabha, B. Bessaïs, H. Ezzaouia, Optical and structural properties of $FeSe_2$ thin films obtained by selenization of sprayed amorphous iron oxide films, Thin Solid Films 511–512 (2006) 457–462.
[49] X. Xu, Y. Ge, M. Wang, Z. Zhang, P. Dong, R. Baines, M. Ye, J. Shen, Cobalt-doped $FeSe_2$-RGO as highly active and stable electrocatalysts for hydrogen evolution reactions, ACS Appl. Mater. Interfaces 8 (2016) 18036–18042.
[50] L. Yan, G. Chen, S. Tan, M. Zhou, G. Zou, S. Deng, S. Smirnov, H. Luo, Titanium oxynitride nanoparticles anchored on carbon nanotubes as energy storage materials, ACS Appl. Mater. Interfaces 7 (2015) 24212–24217.
[51] S. Park, J. An, J.R. Potts, A. Velamakanni, S. Murali, R.S. Ruoff, Hydrazine-reduction of graphite- and graphene oxide, Carbon 49 (2011) 3019–3023.
[52] X. Dai, K. Du, Z. Li, H. Sun, Y. Yang, W. Zhang, X. Zhang, Enhanced hydrogen evolution reaction on few–layer MoS_2 nanosheets–coated functionalized carbon nanotubes, Int. J. Hydrogen Energy 40 (2015) 8877–8888.
[53] Q. Zheng, X. Cheng, H. Li, Microwave synthesis of high activity $FeSe_2$/C catalyst toward oxygen reduction reaction, Catalysts 5 (2015) 1079–1091.
[54] A.P. Grosvenor, B.A. Kobe, M.C. Biesinger, N.S. McIntyre, Investigation of multiplet splitting of Fe 2p XPS spectra and bonding in iron compounds, Surf. Interface Anal. 36 (2004) 1564–1574.
[55] S. Huang, Q. He, W. Chen, Q. Qiao, J. Zai, X. Qian, Ultrathin $FeSe_2$ nanosheets: controlled synthesis and application as a heterogeneous catalyst in dye-sensitized solar cells, Chem. A Eur. J. 21 (2015) 4085–4091.
[56] S. Huang, Q. He, W. Chen, J. Zai, Q. Qiao, X. Qian, 3D hierarchical $FeSe_2$ microspheres: controlled synthesis and applications in dye-sensitized solar cells, Nanomater. Energy 15 (2015) 205–215.
[57] X. Xu, F. Song, X. Hu, A nickel iron diselenide-derived efficient oxygen-evolution catalyst, Nat. Commun. 7 (2016) 12324–12330.
[58] T.W. Lin, C.J. Liu, J.Y. Lin, Facile synthesis of MoS_3/carbon nanotube nanocomposite with high catalytic activity toward hydrogen evolution reaction, Appl. Catal. B Environ. 134–135 (2013) 75–82.
[59] P. Chen, R.L. Mccreery, Control of electron transfer kinetics at glassy carbon electrodes by specific surface modification, Anal. Chem. 68 (1996) 3958–3965.
[60] X. Chia, A.Y.S. Eng, A. Ambrosi, S.M. Tan, M. Pumera, Electrochemistry of nanostructured layered transition-metal dichalcogenides, Chem. Rev. 115 (2015) 11941–11966.
[61] G.A. Mabbott, An introduction to cyclic voltammetry, J. Chem. Educ. 60 (1983) 697–702.
[62] T.W. Swaddle, Homogeneous versus heterogeneous self-exchange electron transfer reactions of metal complexes: insights from pressure effects, Chem. Rev. 105 (2005) 2573–2608.
[63] R. Weerasooriya, H.J. Tobschall, Pyrite-water interactions: effects of pH and pFe on surface charge, Colloids and Surfaces A: Physicochem. Eng. Aspects 264 (2005) 68–74.
[64] D. Fornasiero, V. Eijt, J. Ralston, An electrokinetic study of pyrite oxidation, Colloids Surf. A 62 (1992) 63–73.
[65] J. Bebie, M.A. Schoonen, M. Fuhrmann, D.R. Strongin, Surface charge development on transition metal sulfides: an electrokinetic study, Geochem. Cosmochim. Acta 62 (1998) 633–642 (20) Atieh, M. A.; Bakather, O. Y.; Al-Tawbini, B.; Bukhari, A. A.
[66] F.A. Abuilaiwi, M.B. Fettouhi, Effect of carboxylic functional group functionalized on carbon nanotubes surface on the removal of lead from water, Bioinorgan. Chem. Appl. (2010) 1.
[67] C.J. Madadrang, H.Y. Kim, G. Gao, N. Wang, J. Zhu, H. Feng, M. Gorring, M.L. Kasner, S. Hou, Adsorption behavior of EDTA-graphene oxide for Pb (II) removal, ACS Appl. Mater. Interfaces 4 (2012) 1186–1193.
[68] R.S. Nicholson, I. Shain, Theory of stationary electrode polarography. Single scan and cyclic methods applied to reversible, irreversible, and kinetic systems, Anal. Chem. 36 (1964) 706–723.
[69] D.A.C. Brownson, C.E. Banks, The Handbook of Graphene Electrochemistry, ©Springer-Verlag London Ltd., 2014.
[70] R.S. Nicholson, Theory and application of cyclic voltammetry for measurement of electrode reaction kinetics, Anal. Chem. 37 (1965) 1351–1355.
[71] A.A.A. Aljabali, J.E. Barclay, J.N. Butt, G.P. Lomonossoff, D.J. Evans, P. Lomonossoff, D.J. Evans, Redox-active ferrocene-modified Cowpea mosaic virus nanoparticles, Dalton Trans. 39 (2010) 7569–7574.
[72] Y. Zhang, L. Zuo, L. Zhang, Y. Huang, H. Lu, W. Fan, T. Liu, Cotton wool derived carbon fiber aerogel supported few-layered $MoSe_2$ nanosheets as efficient electrocatalysts for hydrogen evolution, ACS Appl. Mater. Interfaces 8 (2016) 7077–7085.
[73] J. Benson, M. Li, S. Wang, P. Wang, P. Papakonstantinou, Electrocatalytic hydrogen evolution reaction on edges of a few layer molybdenum disulfide nanodots, ACS Appl. Mater. Interfaces 7 (2015) 14113–14122.
[74] J.D. Benck, T.R. Hellstern, J. Kibsgaard, P. Chakthranont, T.F. Jaramillo, Catalyzing the hydrogen evolution reaction (HER) with molybdenum sulfide nanomaterials, ACS Catal. 4 (2014) 3957–3971.
[75] J. Xie, H. Zhang, S. Li, R. Wang, X. Sun, M. Zhou, J. Zhou, X.W. Lou, Y. Xie, Defect-rich MoS_2 ultrathin nanosheets with additional active edge sites for enhanced electrocatalytic hydrogen evolution, Adv. Mater. 25 (2013) 5807–5813.
[76] Y. Li, H. Wang, L. Xie, Y. Liang, G. Hong, H. Dai, MoS_2 nanoparticles grown on graphene: an advanced catalyst for the hydrogen evolution reaction, J. Am. Chem. Soc. 133 (2011) 7296–7299.
[77] B.E. Conway, B.V. Tilak, Interfacial processes involving electrocatalytic evolution and oxidation of H_2, and the role of chemisorbed H, Electrochim. Acta 47 (2002) 3571–3594.
[78] T.W. Lin, C.J. Liu, C.S. Dai, Ni_3S_2/carbon nanotube nanocomposite as electrode material for hydrogen evolution reaction in alkaline electrolyte and enzyme-free glucose detection, Appl. Catal. B Environ. 154–155 (2014) 213–220.
[79] D.J. Li, U.N. Maiti, J. Lim, D.S. Choi, W.J. Lee, Y. Oh, G.Y. Lee, S.O. Kim, Molybdenum sulfide/N-doped CNT forest hybrid catalysts for high-performance hydrogen evolution reaction, Nano Lett. 14 (2014) 1228–1233.
[80] H. Bin Wu, B.Y. Xia, L. Yu, X.-Y. Yu, X.W. (David) Lou, Porous molybdenum carbide nano-octahedrons synthesized via confined carburization in metal-organic frameworks for efficient hydrogen production, Nat. Commun. 6 (2015) 6512–6519.